Replication-timing-correlated spatial chromatin arrangements in cancer and in primate interphase nuclei

Florian Grasser[1], Michaela Neusser[1], Heike Fiegler[2], Tobias Thormeyer[1], Marion Cremer[1], Nigel P. Carter[2], Thomas Cremer[1,3] and Stefan Müller[1,*]

[1]Department of Biology II, Human Genetics, Ludwig-Maximilians University Munich, 82152 Planegg-Martinsreid, Germany
[2]The Wellcome Trust Sanger Institute, Wellcome Trust Genome Campus, Cambridge CB10 1SA, UK
[3]Center for Integrated Protein Science Munich (CIPSM), Ludwig-Maximilians University Munich, Munich, Germany
*Author for correspondence (e-mail: s.mueller@lrz.uni-muenchen.de)

Accepted 17 March 2008
Journal of Cell Science 121, 1876-1886 Published by The Company of Biologists 2008
doi:10.1242/jcs.026989

Summary

Using published high-resolution data on S-phase replication timing, we determined the three-dimensional (3D) nuclear arrangement of 33 very-early-replicating and 31 very-late-replicating loci. We analyzed diploid human, non-human primate and rearranged tumor cells by 3D fluorescence in situ hybridization with the aim of investigating the impact of chromosomal structural changes on the nuclear organization of these loci. Overall, their topology was found to be largely conserved between cell types, species and in tumor cells. Early-replicating loci were localized in the nuclear interior, whereas late-replicating loci showed a broader distribution with a higher preference for the periphery than for late-BrdU-incorporation foci. However, differences in the spatial arrangement of early and late loci of chromosome 2, as compared with those from chromosome 5, 7 and 17, argue against replication timing as a major driving force for the 3D radial genome organization in human lymphoblastoid cell nuclei. Instead, genomic properties, and local gene density in particular, were identified as the decisive parameters. Further detailed comparisons of chromosome 7 loci in primate and tumor cells suggest that the inversions analyzed influence nuclear topology to a greater extent than the translocations, thus pointing to geometrical constraints in the 3D conformation of a chromosome territory.

Supplementary material available online at
http://jcs.biologists.org/cgi/content/full/121/11/1876/DC1

Key words: Nuclear architecture, Replication timing, Chromosome territory, Tumor, Primate

Introduction

DNA replication timing during S phase is correlated with distinct genomic features such as GC content, gene and SINE (short interspersed repeat element) density and high transcriptional activity (Craig and Bickmore, 1993; Dutrillaux et al., 1976; Holmquist et al., 1982; Schwaiger and Schubeler, 2006; Zink, 2006). Recent high-resolution analyses provided a detailed insight into these relationships in yeast, *Drosophila* and man (Cohen et al., 2006; Gregory et al., 2006; Raghuraman et al., 2001; Schubeler et al., 2002; Woodfine et al., 2004; Woodfine et al., 2005). Results in *Drosophila* pointed to a strong correlation between DNA replication in early S phase and transcriptional activity (Schubeler et al., 2002). For human S-phase nuclei from lymphoblastoid cells, the GC level was most significantly correlated with replication timing. In addition, a connection between replication timing and the local gene density, but not with absolute gene expression levels, was observed (Gregory et al., 2006; Woodfine et al., 2004; Woodfine et al., 2005). In another study, Gilbert et al. found a positive correlation between open chromatin conformation and early replication (Gilbert et al., 2004). Taken together, emerging evidence indicates that decondensed chromatin is a distinctive feature of gene-dense genomic regions and might create an environment that facilitates transcription and early replication during S phase.

DNA is replicated in so-called replication foci, which can be visualized by pulse labeling of DNA with thymidine analogs (Taylor et al., 1957). These foci also show a distinct spatiotemporal distribution pattern in the S-phase nucleus (Nakamura et al., 1986). In a wide range of human cell types, DNA that replicates early was preferentially found in the nuclear interior, whereas mid-to-late-replicating DNA was found in the nuclear periphery and around nucleoli, and late-replicating DNA in larger clusters throughout the nucleus (O'Keefe et al., 1992). This three-dimensional pattern of replication foci is evolutionarily highly conserved, having been observed in cells from a wide range of plants and animals (Alexandrova et al., 2003; Dimitrova and Berezney, 2002; Habermann et al., 2001; Mayr et al., 2003; Postberg et al., 2005).

Chromosomes in interphase occupy so-called chromosome territories (CTs), which are spatially arranged according to their gene density or size (for reviews, see Misteli, 2005; Foster and Bridger, 2005; Cremer et al., 2006). An emerging body of evidence indicates that the segmental organization of vertebrate metaphase chromosomes is correlated with a non-random spatial organization of chromatin, resulting in a polarized organization of CTs. For some genes, transcriptional activity could be correlated with a preferential positioning of the locus towards the nuclear interior and/or to the CT surface (for reviews, see Bartova and Kozubek, 2006; Lanctot et al., 2007). Other recent work demonstrated that regional gene density is the decisive parameter determining radial chromatin positioning (Amrichova et al., 2003; Küpper et al., 2007; Neusser

et al., 2007; Sadoni et al., 1999; Goetze et al., 2007; Murmann et al., 2005). In addition, non-random spatial genome arrangements with respect to the local GC content have been discovered for several vertebrate lineages (Saccone et al., 2002; Federico et al., 2004; Federico et al., 2005).

Despite the fact that replication-timing-correlated spatial chromatin arrangements represent an important principle of higher order nuclear architecture, surprisingly little is known about the impact of replication timing on the positioning of defined genomic loci with respect to the nucleus and to the CT surface. By scoring the ratio of singlets/doublets in S-phase nuclei, the replication-timing-dependent spatial arrangement of several human chromosome-12-specific cosmid clones was determined (Nogami et al., 2000), indicating that early-replicating loci were located more internally within the nucleus than were late-replicating loci. Visser et al. observed no differences in the location of early-replication versus mid-to-late-replication foci with respect to the territories of chromosome 8 and the active X chromosome, whereas in the inactive X-chromosome early-replicating chromatin was observed preferentially near the territory surface (Visser et al., 1998).

In the present study, we utilized the high-resolution replication timing data from previous array comparative genomic hybridization (aCGH) (Woodfine et al., 2004) to obtain a set of large-insert clones for very-early-replicating and very-late-replicating loci. We used these clones in 3D-FISH experiments to determine the replication-timing-correlated nuclear topology of over 60 genomic loci in human lymphoblastoid and fibroblast cells. We further analyzed cell lines from several non-human primates and tumor cell lines of human origin, which allowed us to investigate the impact of inversions, translocations and iso-chromosomes on the nuclear positioning of these loci.

Results

In this study we determined the replication-timing-correlated nuclear topology of over 60 loci in established cell lines derived from different human cell types, from human tumors and from non-human primate species. We selected large-insert clones for 3D-FISH experiments that had been previously identified by aCGH to represent very-early-replicating (S:G1 fluorescence intensity ratio >1.9) or very-late-replicating (S:G1 fluorescence intensity ratio <1.15) loci in the human lymphoblastoid cell line CO202 (Woodfine et al., 2004). A summary of all clones used, together with their precise replication timing, local GC content and gene density is given in supplementary material Table S1. Importantly, these clones originated from euchromatic regions of the human genome, excluding pericentromeric, interstitial or subtelomeric regions enriched in segmental duplications or other highly repetitive sequence motifs. We designed several probe pools comprising clones for early-replicating and for late-replicating loci representing (1) all human chromosomes with at least one clone per chromosome and (2) chromosome-specific pools for chromosomes 2, 5, 7 and 17. We selected these four chromosomes because they differ considerably in their replication timing profile, but also in their genomic landscape. Human tumor and non-human primate samples were chosen for comparison with human diploid cells because these four chromosomes were previously found to be involved in various types of structural rearrangements in the respective cell lines. For each FISH experiment, one pool for early-replicating and one pool for late-replicating loci were differentially labeled, combined with the respective chromosome-specific paint probe labeled in a third color, and hybridized to 3D-preserved nuclei from the above-mentioned cell lines.

All 3D-FISH experiments were performed on S-phase cells identified by BrdU pulse labeling, in order to exclude the possible influence of the cell cycle stage on the nuclear positioning of the investigated loci. The observed 3D-FISH patterns were quantitatively evaluated and provided information on the spatial arrangement of these loci with respect to the CT and the nucleus. To obtain further insight into the topology of particular loci, additional 3D-FISH experiments were performed with subsets of clones or with single clones.

Nuclear topology of early-replicating and late-replicating loci with respect to replication foci

We first obtained an overview of the nuclear topology of early-replicating and late-replicating genomic loci with respect to early-replication and late-replication foci. For this purpose, we performed 3D-FISH with two clone pools comprising 21 early-replicating or 19 late-replicating loci (Fig. 1A; supplementary material Table S1A for probe composition). If available, one clone per pool would be representative for each human chromosome. The two clone pools were differentially labeled, combined, and hybridized to diploid human fibroblasts, which were double pulse labeled with BrdU (early S-phase pulse) and with Tamra-dUTP (late S-phase pulse) (Fig. 1B-G). Quantitative 3D evaluation revealed that early-replicating genomic loci were located throughout the nuclear interior to the exclusion of the nuclear border, whereas late-replicating loci showed a broader distribution with preference for the nuclear periphery (Fig. 1K). In addition, late-replicating clones were located significantly more peripherally than were late-replication foci.

In a second set of 3D-FISH experiments using these probe pools, we compared the spatial arrangement of genomic loci in human fibroblast cell nuclei and in the highly rearranged, adherently growing cancer cell lines Mel Juso and SW620, which have rather spherically shaped nuclei (Fig. 1H-J). Again, measurements of absolute distances to the nuclear surface (ADS) of the large-insert clone signals revealed a significant difference between early-replicating and late-replicating loci for nuclei of human fibroblasts, Mel Juso and SW620, regardless of the gross chromosomal rearrangements that occurred in both cancer cell lines (Fig. 1L,M; supplementary material Fig. S1 and Table S2A).

Nuclear topology of chromosome 2 loci

The human chromosome-2-specific clone pools comprised four clones for early-replicating and three clones for late-replicating loci (Fig. 2A; supplementary material Table S1B). Using this probe set in combination with a chromosome-2-specific paint probe, we analyzed human and gorilla lymphoblastoid cell nuclei and human fibroblasts (Fig. 2A-D). Human chromosome 2 is the product of an evolutionary fusion of two ancestral chromosomes still present in the gorilla (supplementary material Fig. S2A). The evaluation of the mean radial distribution yielded no significant differences between early-replicating and late-replicating loci in each experiment, although the shape of the distribution curves for late loci differed between human and gorilla lymphoblastoid cell nuclei (Fig. 2E-G; supplementary material Table S2C). When comparing the radial arrangement between the two human cell types or between human and gorilla lymphoblastoids, again no statistically significant differences were observed for early or for late loci (supplementary material Table S2C).

The absolute distance of early-replicating and late-replicating loci to the chromosome 2 territory surface was also found not to be

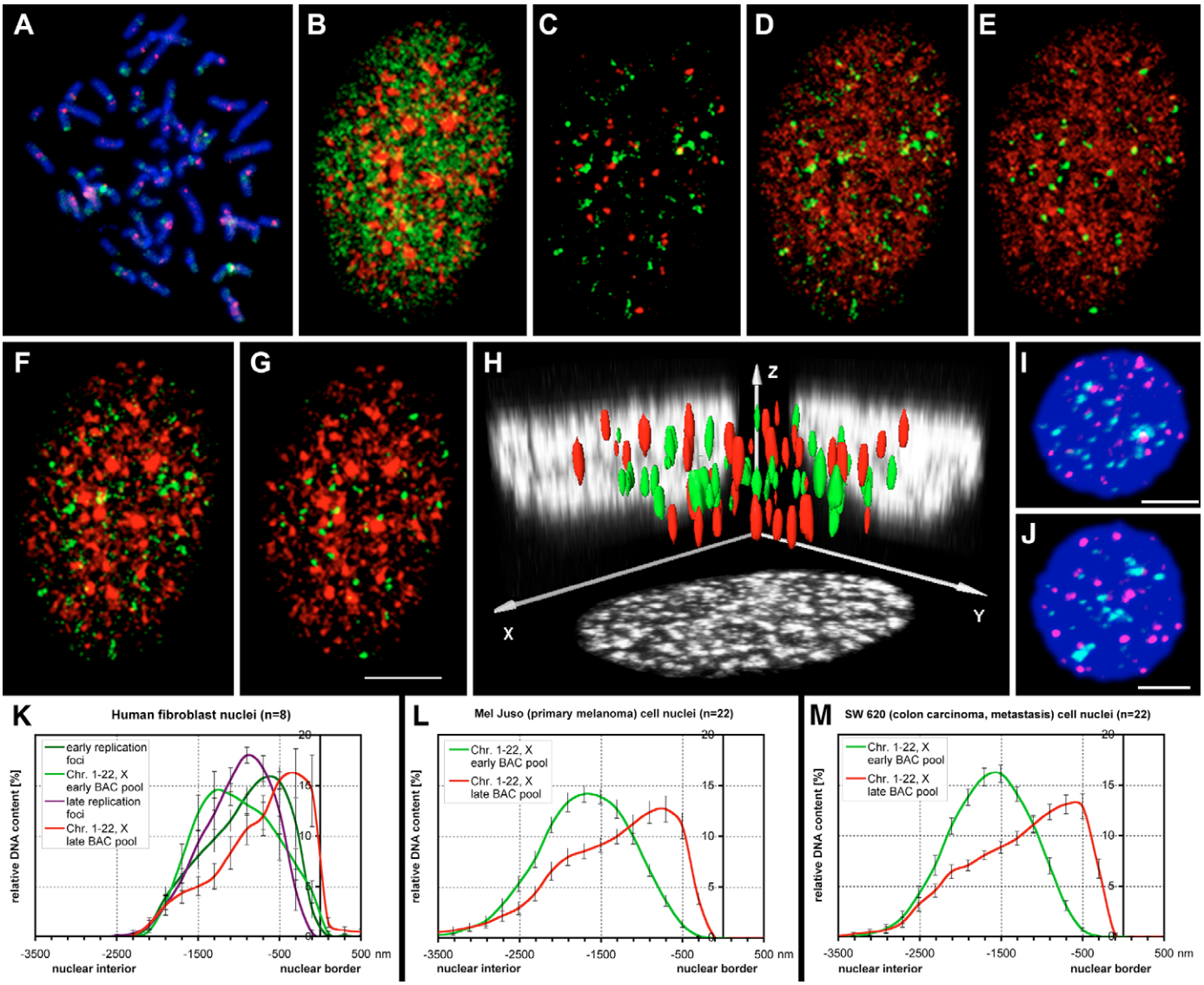

Fig. 1. (A-D) Representative FISH experiments with a two-color clone pool for one early-replicating (green) and/or late-replicating (red) locus per chromosome 1-22 and X. (A) Human metaphase chromosomes. (B-G) Dual-color displays of a representative human fibroblast nucleus (maximum intensity projection) after 3D-FISH of the chromosomes 1-22;X clone pools and double-pulse-labeled replication foci. Scale bar: 5 μm. (B) Early-replication foci in green, late-replication foci in red. (C) Early-replicating clone FISH signals in green, late-replicating clone FISH signals in red. (D) Early-replicating clone FISH signals in green, early-replication foci in red. (E) Late-replicating clone FISH signals in green, early-replication foci in red. (F) Early-replicating clone FISH signals in green, late-replication foci in red. (G) Late-replicating clone FISH signals in green, late-replication foci in red. (H) 3D reconstructed human fibroblast nucleus. (I,J) 3D maximum intensity projections of nuclei from hybridized tumor cell lines Mel Juso and SW620. DAPI counterstain in blue. Scale bar: 5 μm. (K-M) Quantitative evaluation of the radial probe distribution in the nucleus (*n*=number of nuclei) using eADS software for (K) human fibroblasts, together with early-replication and late-replication foci, (L) Mel Juso and (M) SW620.

significantly different in human lymphoblastoid cell and fibroblast nuclei (supplementary material Table S2C). Both early-replicating and late-replicating chromatin was located throughout the CT (Fig. 2H,I).

We further compared the localization of the two late-replicating clones 2-3l and 2-6l, which have similar gene density and GC content, in human fibroblast nuclei. Notably, clone 2-3l was significantly more centrally located than clone 2-6l, exemplifying the fact that each late-replicating locus has a distinct radial positional probability, which may, however, differ considerably between loci (Fig. 2J; supplementary material Table S2C).

Nuclear topology of chromosome 5 and 17 loci

We combined the analysis of human chromosomes 5 and 17 as they represent examples of chromosomes with only very-late-replicating and very-early-replicating loci, respectively (Woodfine et al., 2004). Using differentially labeled pools of late chromosome 5 and early chromosome 17 clones (Fig. 3A; supplementary material Table S1C,E) in combination with the respective painting probes, we investigated human and gorilla fibroblast and lymphoblastoid cell nuclei, gibbon lymphoblastoid cells and cancer cell lines Mel Juso and SW620 (Fig. 3A-F). In the gorilla, these two chromosomes underwent a reciprocal translocation t(5;17),

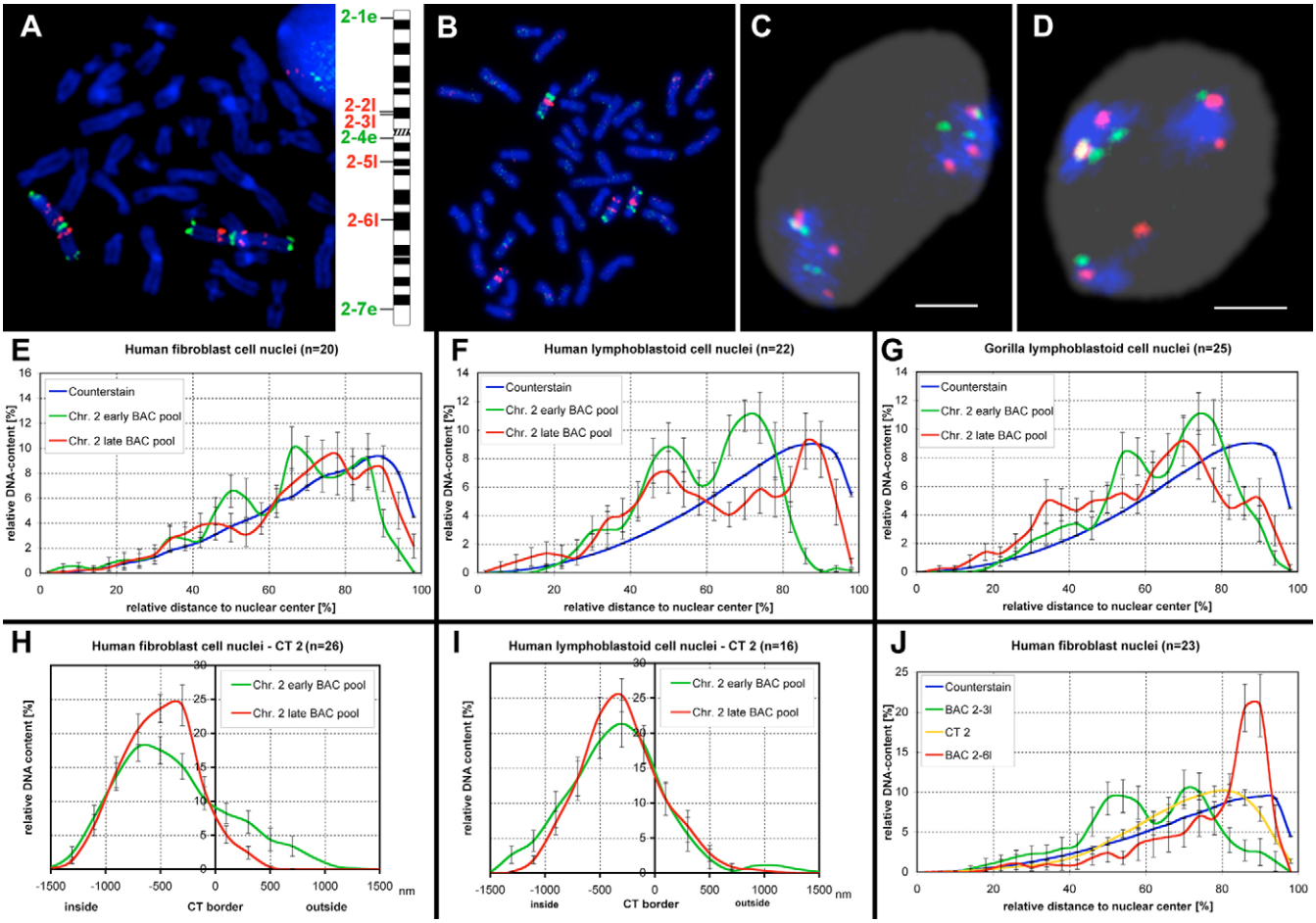

Fig. 2. (A-D) FISH with human chromosome-2-specific pools of large-insert clones representing early-replicating (green) and late-replicating (red) loci to (A) human (schematic of human chromosome 2, together with the mapping position of large-insert clones is shown alongside) and (B) gorilla metaphase chromosomes. (C,D) 3D maximum intensity projections of hybridized human fibroblast and gorilla lymphoblastoid cell nuclei, with early clones labeled green, late clones red, chromosome 2 territories blue and DAPI counterstain gray. Scale bar: 5 µm. (E-J) Quantitative evaluation of radial probe distributions using 3D-RRD or eADS software (*n*=number of nuclei). The distribution of chromosome 2 clone pools (E) in human fibroblasts, (F) in human lymphoblastoid cell nuclei and (G) in gorilla lymphoblastoid cell nuclei. (H,I) The radial probe distribution with respect to the human chromosome 2 territory and (J) the localization of individual clones 2-3l and 2-6l and the chromosome 2 territory in human fibroblast nuclei.

whereas in the Concolor gibbon the chromosome 5 and 17 loci were translocated to three and two gibbon chromosomes, respectively (supplementary material Fig. S2B and Fig. S3A). The cell line Mel Juso showed a derivative chromosome, der(17)t(17;17;17), in addition to a wild-type chromosome 17, whereas in cell line SW620 we focused our analysis on derivative chromosomes der(5;7)(p11;p11) and der(5)t(5;20)(q15;p12) (supplementary material Fig. S3B-D).

In lymphoblastoid cell nuclei of human, gorilla and gibbon, the large-insert clones specific for chromosome 17 early-replicating loci were always located significantly more internally than the clones specific for late-replicating chromosome 5 loci. These differences were most pronounced in human, being somewhat smaller in the gorilla and gibbon. The same was true for human fibroblasts and, to a lesser but still statistically significant extent, for gorilla fibroblasts (Fig. 3G,H; supplementary material Fig. S3E-G and Table S2D).

In the tumor cell lines Mel Juso and SW620, the entire chromosome 5 clone pool, but also the individually hybridized clone 5-1l, showed a peripheral localization in wild-type and in chromosome 5 derivatives (Fig. 3J,K; supplementary material Fig. S3H,I and Table S2D). Remarkably, in Mel Juso cells the der(17) early-replicating loci were significantly more centrally localized than they were in the wild-type chromosome 17, whereas the larger der(17) CT as a whole was significantly more peripherally localized than its wild-type counterpart (Fig. 3I). This observation can be explained by a higher density of early-replicating loci on the der(17) compared with the wild-type chromosome 17, opposing the well-known size-correlated radial arrangement of CTs typical of adherently growing cells (Bolzer et al., 2005; Neusser et al., 2007).

The absolute distance of clones for late-replicating loci to the chromosome 5 territory surface was greater than the distance of the early-replicating clones to the chromosome 17 territories. Absolute distance measurements in the two reciprocal translocation products, t(5;17), in gorilla extended these findings. Both in the small and the large translocation product, the early-replicating loci were located significantly closer to the territory surface, with a considerable amount of early-replicating chromatin located outside

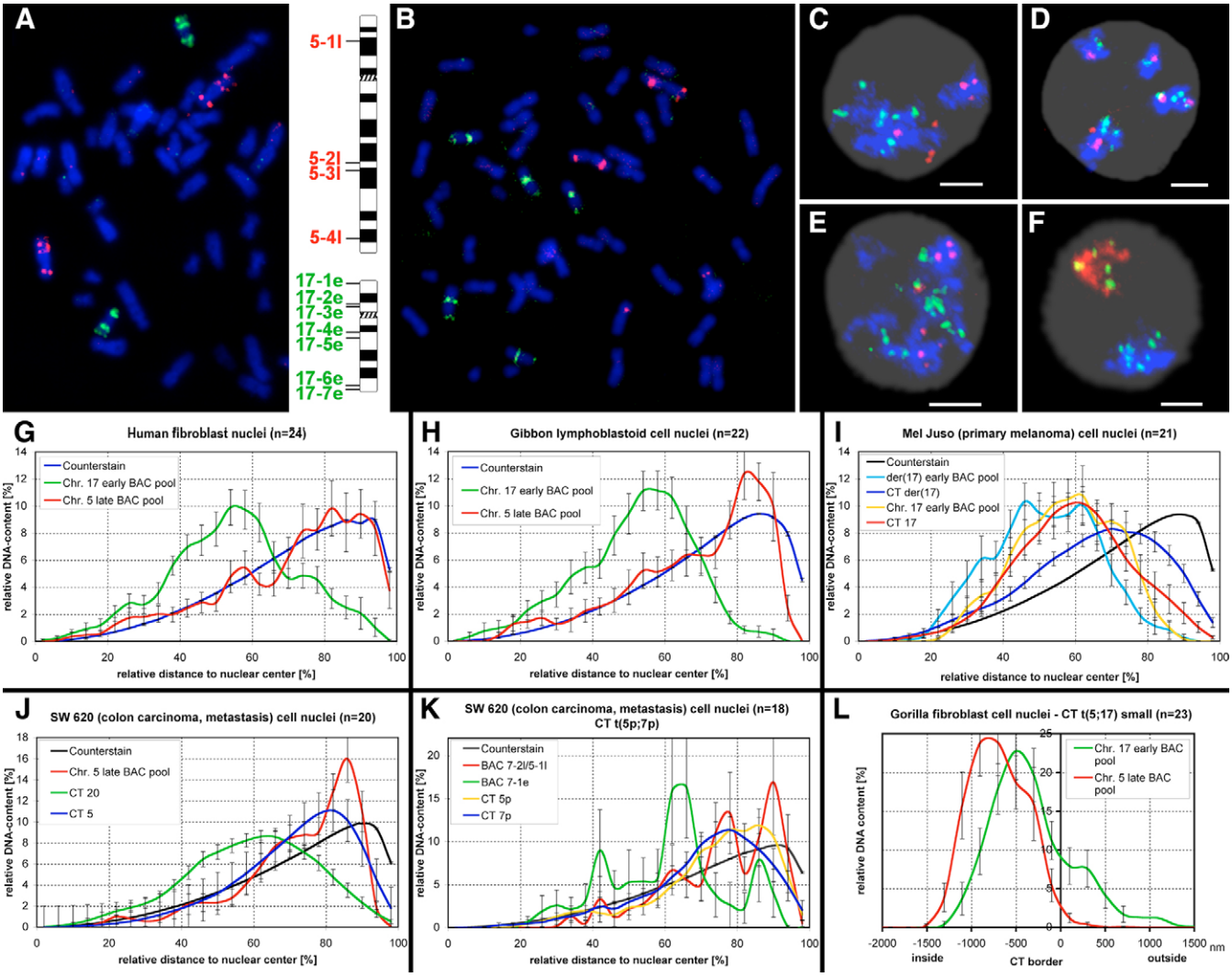

Fig. 3. FISH with pooled large-insert clones representing chromosome 17 early-replicating (green) and chromosome 5 late-replicating (red) loci to (A) human (schematics of human chromosomes 5 and 17, together with the mapping position of large-insert clones, are shown alongside) and (B) Concolor gibbon metaphase chromosomes. 3D maximum intensity projections of nuclei from (C) human, (D) gorilla, (E) Concolor gibbon lymphoblastoids and (F) Mel Juso tumor cells hybridized with these probe pools. In C-F, chromosome 17 early-replicating clones are labeled green, chromosome 5 late-replicating clones red, chromosome 5 and 17 territories blue and DAPI counterstain gray, except for F, in which the wild-type CT17 is shown in blue and the CT der(17) in red. Scale bar: 5 μm. (G-L) Quantitative evaluation of radial probe distributions in the interphase nucleus or the respective chromosome territory, using 3D-RRD or eADS software (*n*=number of nuclei).

the core territory (Fig. 3L; supplementary material Fig. S3J,K and Table S2D).

Nuclear topology of chromosome 7 loci

Differentially labeled large-insert clone pools for two early-replicating and four late-replicating loci (supplementary material Table S1D) were hybridized together with a chromosome 7 paint to lymphoblastoid cell nuclei of human, gorilla and Concolor gibbon, to human fibroblasts and to cancer cell lines Karpas 384 and Mel Juso (Fig. 4A-D,F,G; supplementary material Fig. S4A,B). We further compared the nuclear positioning of five individual clones in human and orangutan fibroblasts (Fig. 4E,H). Among the great apes, chromosome 7 has evolved by a pericentric and a paracentric inversion. The orangutan is characterized by the ancestral chromosome 7 homolog with both inversions, whereas humans display the evolutionarily derived chromosome 7, and in the Concolor gibbon the ancestral chromosome 7 form has been translocated (supplementary material Fig. S2C). The cancer cell line Mel Juso displays a iso(7p) and cell line Karpas 384 a der(7)del(7)(p13)inv(7)(p13;q22.1) (supplementary material Fig. S4C,D).

For all FISH experiments with chromosome clone pools, quantitative evaluation of the 3D relative radial distribution revealed a significantly more internal nuclear localization of early-replicating loci than of late-replicating loci, irrespective of cell type, species or tumor type (Fig. 4I,J; supplementary material Fig. S4E,F and Table S2E). However, at closer inspection, differences were found when comparing the homologs of the different primates. Orangutan and gibbon showed very similar distribution curves with a single maximum, indicating that translocations to three different chromosomes in the gibbon did not result in changes to the nuclear topology. By contrast, two distribution maxima were observed in

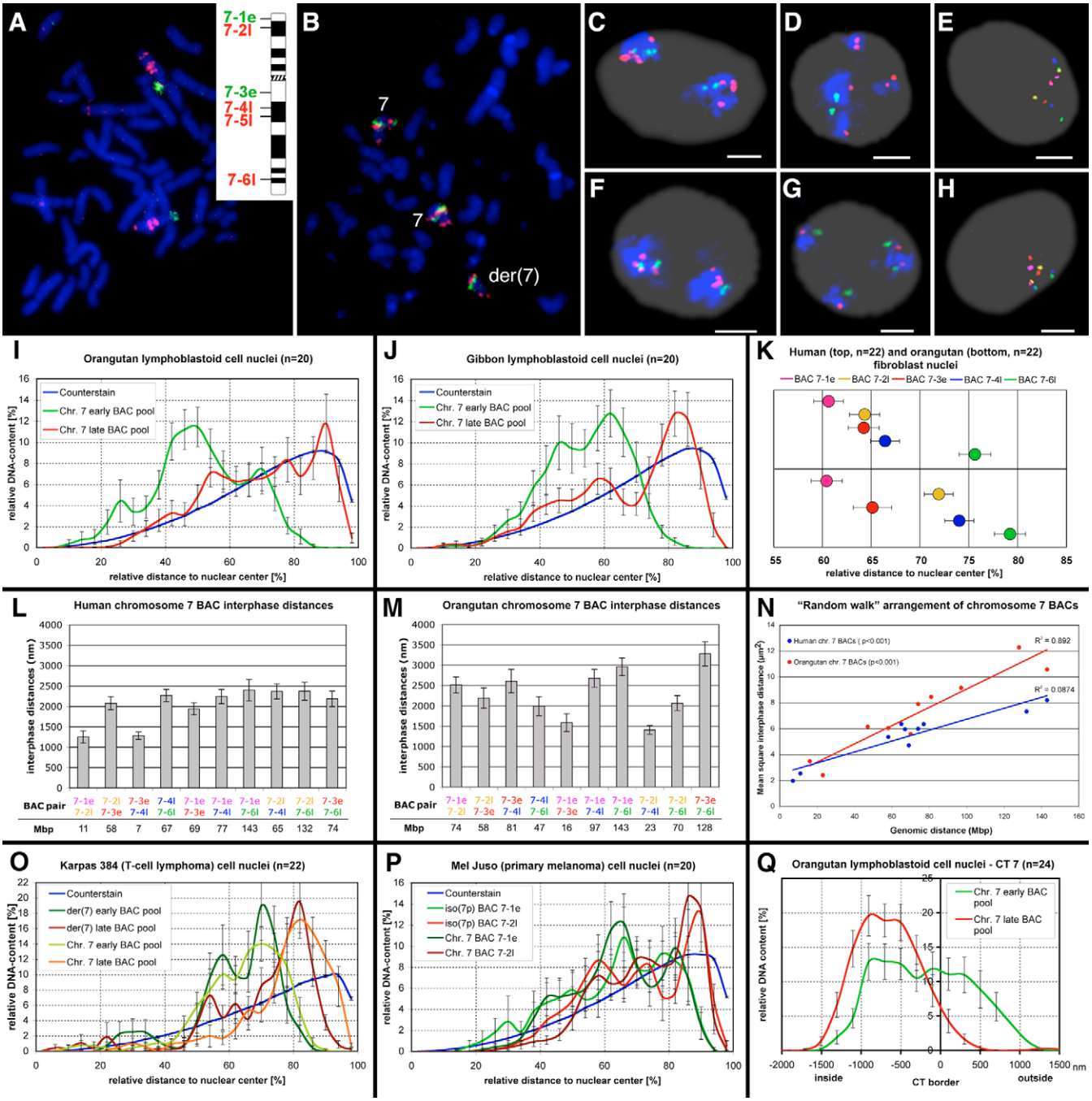

Fig. 4. Representative (A) orangutan (schematic of human chromosome 7, together with the mapping position of large-insert clones, is shown alongside) and (B) Karpas 384 metaphases after FISH with human chromosome-7-specific pools of large-insert clones representing early-replicating (green) and late-replicating (red) loci. (C,D,F,G) 3D maximum intensity projections of nuclei from (C) human fibroblasts, (D) Concolor gibbon lymphoblastoids, (F) orangutan lymphoblastoids and (G) Mel Juso cells hybridized with the early-replicating clone pool labeled green, the late-replicating clone pool in red, chromosome 7 territories blue and DAPI counterstain gray. (E) Human and (H) orangutan *z*-projected fibroblast nuclei after multicolor 3D-FISH with five BAC clones. The clone color code follows panel K. Scale bar: 5 µm. (I-K,O-Q) Quantitative evaluation of radial probe distributions in the interphase nucleus or the respective chromosome territory, using 3D-RRD or eADS software (*n*=number of nuclei). (L,M) Mean pair-wise clone distance measurements in human and orangutan fibroblast nuclei from the 3D-FISH experiments illustrated in E,H,K. (N) In both species the mean square interphase distance between two clone loci showed a linear correlation with their genomic distance, indicating a 'random walk' 3D conformation of these loci.

human nuclei. The human and orangutan graphs apparently reflect the mapping position of early-replicating and late-replicating regions along chromosome 7 homologs: human chromosome 7 displays alternating positions of early-replicating and late-replicating loci on both the p- and q-arms, whereas in the orangutan both early-replicating loci are located on the p-arm.

To further investigate the potential correlation between metaphase chromosome organization and interphase CT topology, six-color

FISH experiments were performed on fibroblast nuclei of human and orangutan with differentially labeled clones 7-1e, 7-2l, 7-3e, 7-4l and 7-6l. In orangutan nuclei, the mean average relative radius (ARR) values clearly followed the order of the five clones on metaphase chromosome 7, with the two early-replicating p-arm loci pointing towards the nuclear center (Fig. 4K). The most-distal clones from each chromosome arm that were not affected by the inversions showed rather conserved ARR values in both species. Clone 7-3e, representing an early-replicating but inverted locus, also maintained its approximate positioning, whereas clones 7-2l and 7-4l for late-replicating and inverted loci differed considerably in their positioning between the two species.

Three-dimensional interphase distance measurements between these five clones in human and orangutan provided further evidence for nuclear repositioning of evolutionarily inverted loci (Fig. 4L,M). For example, the mean interphase distances for clone pairs 7-1e/7-2l and 7-3e/7-6l were greater in orangutan. Correspondingly, the 3D distances between clones 7-1e/7-3e and 7-2l/7-4l were reduced in orangutan. Furthermore, the overall 3D conformation differed, as is evident from the mean interphase distance difference of over 500 nm between the most distal and evolutionarily conserved clone pair 7-1e/7-6l in human as compared with orangutan. For chromosome 7 of both species, we observed a highly significant correlation between the mean square interphase distance and the genomic distance of any two tested loci (Fig. 4N). The measured interphase distances fully conform with the proposed 'random walk' model of the 3D higher order architecture of CTs (Yokota et al., 1995), although overall, human chromosome 7 is more compacted than its orangutan homolog.

From both the radial arrangement and the distance measurements we conclude that orangutan chromosome 7 shows a straight 3D conformation that is very similar to the linear metaphase chromosome organization, whereas the homologous human loci are arranged in a more compact way. Furthermore, these results demonstrate that late-replicating loci in particular are prone to nuclear repositioning by evolutionary inversions, and suggest that geometrical constraints apply within the 3D interphase CT structure that prevent evolutionarily inverted loci to maintain their original nuclear positioning.

As for evolutionary inversions, the presence of a der(7)del(7)(p13)inv(7)(p13;q22.1) chromosome in the tumor cell line Karpas 384 could be correlated with a statistically significant positional shift of late-replicating loci towards the nuclear center in the der(7) as compared with the wild-type chromosome, whereas the more central location for early-replicating loci remained stable (Fig. 4O; supplementary material Table S2E). By contrast, in the cell line Mel Juso, the duplicated p-arms of the iso-chromosome 7p maintained their polar orientation with clone 7-1e being more centrally located than clone 7-2l (Fig. 4P; supplementary material Table S2E), indicating that the radial positioning of the two identical arms is mirrored and unchanged, as compared with the wild-type chromosome 7p.

Regarding the arrangement with respect to the chromosome 7 territory surface, early-replicating and late-replicating loci showed very similar positioning in human lymphoblastoid and fibroblast nuclei. By contrast, in the orangutan chromosome 7 homolog, where both early clones 7-1e and 7-3e map to the ~20 Mb p-arm, highly significantly smaller ADS values were obtained for the two early-replicating loci than for the late-replicating loci (supplementary material Table S2E). In addition, in orangutan the two clones representing early-replicating loci showed a much stronger tendency to be located outside the core territory than did the four clones representing late-replicating loci (Fig. 4Q), which was not observed in human nuclei (supplementary material Fig. S4I,J).

Discussion

We performed a quantitative analysis of the replication-timing-correlated nuclear topology of 64 loci in lymphoblastoid cell lines and cultivated fibroblasts from human, non-human primates and from cancer cell lines. Collectively, our results demonstrate the preferential interior location with exclusion from the nuclear periphery for very-early-replicating loci, irrespective of cell type or species analyzed. By contrast, very-late-replicating loci were found to be located throughout the nucleus, with preference for the nuclear periphery. However, these positional differences were more pronounced for chromosome 5, 7 and 17 loci than for chromosome 2 loci. In addition, our data showed that evolutionary and cancer-related chromosome translocations appeared to change the nuclear topology of associated loci to a lesser extent than inversions. Finally, both early-replicating and late-replicating loci were found to be located at the surface as well as in the interior of a CT. Exceptions were early-replicating loci from extended gene-dense regions, which were significantly enriched in the proximity of the CT border.

Does replication timing determine the nuclear positioning of a locus?

Our 3D-FISH experiments on human lymphoblastoid cells (Fig. 2; supplementary material Figs S3, S4) were carried out with the cell line CO202, for which genome-wide replication timing had been previously determined by aCGH (Woodfine et al., 2004). In this cell line, we found chromosome-specific differences when comparing the spatial arrangement of early-replicating and late-replicating loci: marginal differences for chromosome 2, but highly statistically significant for chromosome 7 and 5/17 (supplementary material Table S2). These results are hard to explain under the assumption that replication timing of a locus is a major determinant for its nuclear positioning. Considering our experimental design, in which clones were selected for early and late loci with near-identical replication timing (supplementary material Table S1), one would have expected pronounced differences between early-replicating and late-replicating loci for all chromosomes and a well-defined nuclear compartment for the localization of late-replicating loci.

Besides replication timing, genomic properties such as local gene density and GC content have also been suggested as causes for the non-random nuclear positioning of a locus [see Küpper et al. (Küpper et al., 2007) and references therein]. We therefore determined the local gene density and GC content for each of the 64 loci (supplementary material Table S1). As expected, a clear positive correlation was observed between the three factors, with early-replicating loci showing a higher variability in gene density (10.5-57 genes/Mb) and GC content (GC=41.3-56.5%) compared with late-replicating loci (0-7.5 genes/Mb; GC=34.6-38.8%). Most importantly (and as illustrated in supplementary material Fig. S5), the gene density differences of clones chosen for chromosome 2 loci (20:6 genes/Mb in early:late clones, a 3.3-fold difference) were less pronounced than those for chromosome 5/17 (30:3 genes/Mb in early:late clones a 10-fold difference) and 7 (18:3 genes/Mb in early:late clones, a 6-fold difference). This relatively high local gene density of chromosome 2 late-replicating loci best explains their more central nuclear localization. Conversely, clone 2-7e originated from a region of unusually low GC content (42.9% compared with

the average GC content of 50.1%) for early-replicating loci, which might be correlated with a more peripheral localization of the chromosome 2 early-replicating clone pool (ARR=59.3%) compared with those of chromosomes 7 and 17.

These results clearly show – at least for human lymphoblastoid cells in the first instance – that replication timing is not a major factor in the determination of the spatial nuclear positioning of a locus. Instead, our results point towards local gene density, and possibly GC content, as the key players influencing radial nuclear positioning of a locus. The same conclusion was reached by a recently published study from our laboratory, focusing on the nuclear positioning of gene-dense and gene-poor, as well as of transcriptionally active and inactive genomic regions (Küpper et al., 2007). According to this study, the highest correlation coefficient was obtained between nuclear localization and local gene density, followed by the local GC content, whereas the local gene expression level, in particular, was found to be insignificant. In addition, Gilbert et al. excluded the transcriptional activity of single genes and instead emphasized high gene density as deterministic for an open chromatin conformation (Gilbert et al., 2004).

Provided that transcriptional activity plays an important role in the replication timing of a gene, switches in replication timing might be expected for certain tissue-specific genes, which in turn might affect their nuclear positioning in different cell types. Indeed, Hiratani et al. reported changes in the replication timing of a small fraction of tissue-specific genes residing within AT-rich isochores, when mouse embryonic stem cells were compared before and after differentiation (Hiratani et al., 2004). In agreement with this study, the comparison of replication timing of human chromosome 22 in fibroblasts and lymphoblastoid cells by aCGH revealed that over 99% of chromosome regions replicated at the same time in both cell types, despite pronounced differences in gene expression (White et al., 2004). Although locus-specific changes in replication time have been shown for a few additional genes (e.g. Englmann et al., 2005; Cimbora et al., 2000), it is generally assumed that only changes in transcriptional activity over extended genomic regions can influence replication time (Schwaiger and Schubeler, 2006). Concerning the putative influence of species-specific replication timing on the nuclear topology of orthologous genes – possibly connected to differential transcriptional activity – expression profiling of African great ape fibroblasts showed that only about 0.005% of transcripts vary between these species (Karaman et al., 2003). In addition, comparative replication banding analysis of great ape metaphase chromosomes revealed no differences in replication timing of homologous chromosome regions (Weber et al., 1986). In summary, published evidence argues against widespread cell-type or species-specific changes in replication timing.

aCGH analysis would have unequivocally allowed us to determine the precise replication timing profile of all 64 loci in the nine other cell lines used here; however, these experiments are beyond the scope of our present study. Since we have not performed these experiments, we cannot exclude with certainty that the cell-type-, species- or chromosome-specific changes in the nuclear topology patterns of the 64 investigated loci we will discuss below are accompanied by replication timing switches of the respective loci. Nonetheless, considering the published estimate of a frequency of replication timing switches of ~1%, we can infer that the probabilistic chance for replication timing switches of the investigated loci is very small. We can further exclude the possibility that we might have analyzed loci belonging to a recently discovered class of PAN-S-phase loci – loci showing no distinct replication timing because of asynchronous replication (Jeon et al., 2005; Karnani et al., 2007), because these loci would be classified as mid-replicating by aCGH.

Nuclear topology of clone loci compared with replication foci

We combined 3D-FISH of genome-wide large-insert clone pools with double pulse S-phase replication labeling to enable a direct and quantitative comparison of the radial arrangement of early-replication and late-replication foci with the nuclear distribution of early-replicating and late-replicating clone loci in human fibroblast nuclei (Fig. 1). As previously described, both early-replication foci and early-replicating clone loci appear to be excluded from the nuclear periphery. By contrast, late-replication foci showed a significantly more central positioning than large-insert clones representing late-replicating genomic regions. Since no clones used in our study map to regions of late-replicating constitutive heterochromatin, it can be speculated that late-replicating chromatin comprises at least two genomic fractions with distinctly different nuclear distribution patterns, presumably of constitutively heterochromatic and euchromatic origin, respectively. To this end, a more detailed analysis of the nuclear organization of late-replicating euchromatic, facultatively and constitutively heterochromatic loci from different genomic environments would help to establish better-defined rules for the nuclear address of late-replicating chromatin.

Global patterns of nuclear locus positioning

We then compared the radial arrangement of clones for chromosome 2, 5, 17 and 7 early-replicating and late-replicating loci in various cell lines (Figs 2-4). In each of these experiments, early-replicating loci were positioned more centrally and away from the nuclear envelope than were late-replicating loci, in agreement with previous work in which the same polar orientation was observed for human chromosome 12 loci (Nogami et al., 2000). In addition, pooled probes for late-replicating loci yielded broader distribution curves with a distinct peak in the nuclear periphery. This finding was further supported by the strikingly different nuclear positions of individual late-replicating clones 2-3l and 2-6l (Fig. 2J), indicating that late-replicating loci are more variable in their individual positional probability. Neither species, cell type, nor nuclear morphology had any substantial influence on this polar nuclear orientation of early-replicating and late-replicating loci.

Locus positioning within a chromosome territory

We further determined the radial positioning of chromosome 2, 5, 7 and 17 loci with respect to their CT. Early-replicating and late-replicating loci from chromosomes 2 and 7 were found equally distributed throughout the CT in human cells. By contrast, in the reciprocally translocated chromosome t(5;17) homologs of gorilla, and in the inverted chromosome 7 homolog in orangutan, early-replicating chromatin was located close to the CT surface and late-replicating chromatin significantly more to the interior. These distribution differences can be explained by the species-specific presence of extended regions with opposite genomic properties. In gorilla, the two t(5;17) translocation products are each composed of a contiguous gene-dense chromosome 17 and a gene-poor chromosome-5-homologous segment. The same situation is found in the chromosome 7 homolog of orangutan, where the entire ~20 Mb p-arm is gene dense, whereas evolutionary inversions have disrupted this extended genomic region in human chromosome 7.

In summary, only gene-dense regions of several Mb yielded a significantly more external CT position for early-replicating chromatin as compared with late-replicating loci. Even for these genomic regions, extensive looping out from the CT was not observed, as previously shown for the human MHC locus (Volpi et al., 2000), as well as for some other genes (Chambeyron and Bickmore, 2004; Williams et al., 2002; Mahy et al., 2002). Our own results are more comparable with those obtained for early-replication and late-replication foci (Visser et al., 1998), as well as for gene-dense and gene-poor regions or for highly and poorly expressed loci from chromosomes 12, 18 and 19 (Küpper et al., 2007), which were predominantly found distributed throughout the respective CT. Thus, an obviously polar radial organization of individual loci within a CT might not be a common principle, but rather a rare phenomenon characteristic for some extended gene-dense genomic regions or for certain highly expressed genes.

Chromosomal rearrangements and the 3D conformation of chromosome territories

Next, we analyzed the effects of various types of evolutionary and tumor-associated chromosomal rearrangements on nuclear topology. The evolutionary fusion of human chromosome 2 did not significantly change the positioning of early-replicating and late-replicating loci. Likewise, simple reciprocal translocations, such as the evolutionary t(5;17) in gorilla, but also complex translocations of human chromosome 7 homologs in gibbon, only had a moderate effect on the nuclear topology of the rearranged genomic loci. The polar nuclear positioning of loci of the iso-chromosome 7p in the melanoma cell line was equally preserved. From these and previously published studies on the nuclear positioning of translocation chromosomes (Cremer et al., 2003; Neusser et al., 2007; Croft et al., 1999) it can be concluded that the relative nuclear orientation of individual loci within the newly formed CT is largely maintained. This can be best explained by the fact that a translocation only generates a single new neighborhood per CT around the breakpoint, acting as a hinge around which the two subterritories are free to rotate until they reach their original relative nuclear orientation.

In contrast to translocations, the two evolutionary chromosome 7 inversions influenced the nuclear arrangement of inverted loci. Comparing human and orangutan homologs, late clones 7-2l and 7-4l were repositioned, whereas early clones 7-1e and 7-3e remained orientated towards the nuclear center. To a similar extent, the chromosome 7 inversion in the tumor cell line Karpas 384 was accompanied by a positional change of late-replicating loci, whereas the early-replicating clone pool maintained its relative positioning. In support of these results, the 3D conformation of chromosome 7 homologs in human and orangutan was clearly species-specific (Fig. 4K-N). Changes in the genomic distance between two clones caused by evolutionary inversions were always correlated with altered interphase distances, for example between clones 7-3e and 7-4l, or between 7-2l and 7-4l, arguing for nuclear repositioning of inverted loci and against the evolutionary conservation of specific proximities between the investigated loci during interphase. Nevertheless, the human chromosome 7 territory was also more compacted than its orangutan counterpart (Fig. 4N), indicating that the orangutan chromosome 7 territory organization reflects the linear metaphase chromosome structure, whereas the proximal region of the human chromosome 7 showed considerable back-folding in interphase.

Compared with translocations with only one breakpoint per chromosome, inversions require two breaks in a single CT, potentially leading to local changes in genomic properties in both breakpoint-flanking neighborhoods. We hypothesize that rotation of two of these segments might be hindered by opposing forces from the third chromosome segment in the case of an inversion. This implies the presence of geometrical constraints limiting the freedom of genomic loci to maintain their original nuclear positioning after inversions, and to a greater extent than after translocations. A detailed analysis of the nuclear topology of loci flanking evolutionary inversion breakpoints is certainly warranted in light of the fact that over 20 large inversions occurred during the evolution of the great apes (for a review, see Müller, 2006).

In conclusion, from this and other recent studies a common theme emerges, pointing towards local properties of the primary DNA sequence as a major cause for the radial nuclear localization of a locus. Accordingly, high gene density, high GC content and an open chromatin conformation of a genomic region with central nuclear localization might promote transcriptional activity and early replication. By contrast, replication timing and high expression levels of a gene, although, interestingly, intimately correlated with each other (for a review, see Chakalova et al., 2005), do not seem to play a significant role in establishing 3D genome organization, at least not in human lymphoblastoid cell nuclei. It can be speculated that the most probable scenario for the existing nuclear compartmentalization of the genome would be the temporal and spatial coordination of cellular processes such as DNA replication and transcription.

Materials and Methods

Cell material and fixation

Epstein-Barr-virus-immortalized lymphoblast cells, established from peripheral lymphocytes, were used from human [CO202, ECCAC no. 94060845 (Woodfine et al., 2004)], gorilla [EB (JC), ECACC no. 89072703], orangutan (EB185, ECACC no. 89072705) and Concolor gibbon. Primary human, gorilla and orangutan fibroblasts obtained from early passages of skin biopsies were as described previously (Neusser et al., 2007). All lymphoblastoid and fibroblast cells were karyotypically normal. Tumor samples included the established human cell lines Karpas 384, derived from T-cell lymphoma (Dyer et al., 1993), Mel Juso, a melanoma-derived cell line, and SW620 (ATCC no. CCL-227), derived from a metastasis of a colon adenocarcinoma. The karyotypes of Mel Juso and SW620 are described elsewhere (Müller et al., 2004).

To detect S-phase nuclei, cells were pulse labeled with 5-bromodeoxyuridine (BrdU, 10 μM/ml) for 1 hour before fixation. For double pulse labeling of unsynchronized human fibroblasts with the aim of simultaneously visualizing early-replication and late-replication foci, cells were first labeled with BrdU (10 μM) for 2 hours, briefly rinsed in two changes of 1×PBS, then chased in DMEM medium containing 15% FCS for 2 hours and finally scratch-labeled with Tamra-dUTP (Schermelleh et al., 2001) for 2 hours before fixation. Three-dimensional (3D) preserved nuclei were prepared as described (Solovei et al., 2002). Briefly, lymphoblastoids and Karpas 384 cells were fixed in 4% paraformaldehyde in 0.3×PBS; fibroblasts, Mel Juso and SW620 were fixed in 4% paraformaldehyde in 1×PBS. Sequential permeabilization steps included treatment with 0.5% Triton X-100 in 1×PBS; 20% glycerol in 1×PBS; repeated freezing/thawing in liquid nitrogen, incubation in 0.1 M HCl; and pepsinization (2 mg/ml pepsin in 0.01 M HCl at 37°C).

Probe preparation and fluorescence in situ hybridization (FISH)

The painting probes delineating human chromosomes 2, 5, 7 and 17 were amplified and labeled by DOP-PCR as described (Müller et al., 2004). Large-insert clones used in 3D-FISH experiments for the delineation of early and late loci were derived from the 1 Mb clone set previously used in array-CGH experiments for the assessment of replication timing of human lymphoblastoid cells (Woodfine et al., 2004). DNA was labeled by DOP-PCR using primers DOP-2 and DOP-3 (Fiegler et al., 2003). Paint probes and clones were labeled with biotin-dUTP (Roche), digoxigenin-dUTP (Roche), dinitrophenol-dUTP (DNP, NEN Life Science), TAMRA-dUTP (formerly available from PE Applied Biosystems) or Texas Red-dUTP (Molecular Probes). Subsequently, clones for early-replicating and late-replicating loci were pooled to assemble pools specific for human chromosomes 2, 5, 7 and 17 as well as a probe for chromosomes 1-22 and X, as detailed in supplementary material Table S1. One microgram of chromosome-specific chromosome paint and 3 μg of pooled large-insert clone DNA were used together with 30 μg human Cot-1 DNA (Gibco BRL) and 50 μg salmon sperm DNA (Sigma) per 8 μl hybridization mixture.

Biotinylated probes were detected with avidin-Alexa 488 (Molecular Probes) or avidin-Cy5 (Dianova). DNP-labeled probes were visualized by sequential detection

with rabbit anti-DNP and goat anti-rabbit-Alexa 488 (Sigma), or goat anti-rabbit-Alexa 514 (Molecular Probes) antibodies. Digoxigenin-labeled probes were detected with mouse anti-digoxigenin-Cy5 (Dianova). Metaphase chromosomes and 3D fixed interphase nuclei were counterstained for 10 minutes with DAPI (2 μg/ml), or with 1 μM ToPro-3 (Molecular Probes). Detection of incorporated BrdU was performed as described (Solovei et al., 2002).

Digital microscopy and image processing

Metaphase FISH images were captured with a cooled CCD camera (Photometrics C250/A equipped with a Kodak KAF1400 chip) coupled to a Zeiss Axiophot microscope, using SmartCapture VP software (DigitalScientific). Light-optical serial sections of nuclei studied in two- and three-color 3D-FISH experiments were obtained with a laser-scanning confocal microscope (LSM 410. Carl Zeiss MicroImaging) equipped with Ar and He/Ne lasers. For imaging of multicolor 3D-FISH experiments, a Leica TCS SP2 laser-scanning confocal microscope (Leica Microsystems) with beam-splitters tuned for DAPI, FITC, Alexa 514, TAMRA, Texas Red and Cy5 was used. Nuclei were scanned with an axial distance of 200 nm between consecutive light-optical sections yielding separate stacks of 8-bit grayscale images for each fluorescence channel with a pixel size of 60-120 nm. For each optical section, images were collected sequentially for all fluorochromes, followed by correction of the axial chromatic shift for each channel. Image stacks were processed with ImageJ software (http://rsb.info.nih.gov/ij). 3D reconstructions of hybridized nuclei were performed using Amira 4 software (Mercury CS).

Quantitative 3D evaluation of probe distributions

Quantitative 3D evaluation of light-optical serial sections was performed using voxel-based software algorithms 3D-RRD (Three-Dimensional Relative Radius Distribution) (Cremer et al., 2001), eADS (enhanced Absolute 3D Distances to Surfaces) (Küpper et al., 2007) and DistAngle (Distances and Angles). 3D-RRD software was used to quantify the relative radial distribution (% values) of large-insert clone hybridization signals and of chromosome territories (CTs) with respect to the nucleus. Based on the relative radial probe distribution, the average relative radius (ARR; % values) was calculated. eADS software was used to determine the shortest distances (in nm) between clone signals and the nuclear border and with the surface of the corresponding CT. DistAngle was used to measure 3D distances and angles between geometrical centers (centroids) of different probes employing a user-set threshold and the voxel dimensions. To test the data set for significant differences ($P \leq 0.05$), the Mann-Whitney Rank Sum Test (U-Test) was applied on the results of the quantitative evaluation programs described above.

This work was supported by the Deutsche Forschungsgemeinschaft, grant MU 1850/2-1, the Wilhelm-Sanderstiftung, grant 2001.079.2, and the Wellcome Trust Sanger Institute. We thank Dr Abraham Karpas, Department of Haematology, University of Cambridge, UK, for providing the cell line Karpas 384.

References

Alexandrova, O., Solovei, I., Cremer, T. and David, C. N. (2003). Replication labeling patterns and chromosome territories typical of mammalian nuclei are conserved in the early metazoan Hydra. *Chromosoma* **112**, 190-200.

Amrichova, J., Lukasova, E., Kozubek, S. and Kozubek, M. (2003). Nuclear and territorial topography of chromosome telomeres in human lymphocytes. *Exp. Cell Res.* **289**, 11-26.

Bartova, E. and Kozubek, S. (2006). Nuclear architecture in the light of gene expression and cell differentiation studies. *Biol. Cell* **98**, 323-336.

Bolzer, A., Kreth, G., Solovei, I., Koehler, D., Saracoglu, K., Fauth, C., Müller, S., Eils, R., Cremer, C., Speicher, M. R. et al. (2005). Three-dimensional maps of all chromosomes in human male fibroblast nuclei and prometaphase rosettes. *PLoS Biol.* **3**, e157.

Chakalova, L., Debrand, E., Mitchell, J. A., Osborne, C. S. and Fraser, P. (2005). Replication and transcription: shaping the landscape of the genome. *Nat. Rev. Genet.* **6**, 669-677.

Chambeyron, S. and Bickmore, W. A. (2004). Chromatin decondensation and nuclear reorganization of the HoxB locus upon induction of transcription. *Genes Dev.* **18**, 1119-1130.

Cimbora, D. M., Schubeler, D., Reik, A., Hamilton, J., Francastel, C., Epner, E. M. and Groudine, M. (2000). Long-distance control of origin choice and replication timing in the human beta-globin locus are independent of the locus control region. *Mol. Cell. Biol.* **20**, 5581-5591.

Cohen, S. M., Furey, T. S., Doggett, N. A. and Kaufman, D. G. (2006). Genome-wide sequence and functional analysis of early replicating DNA in normal human fibroblasts. *BMC Genomics* **7**, 301.

Costantini, M., Clay, O., Auletta, F. and Bernardi, G. (2006). An isochore map of human chromosomes. *Genome Res.* **16**, 536-541.

Craig, J. M. and Bickmore, W. A. (1993). Chromosome bands: flavours to savour. *BioEssays* **15**, 349-354.

Cremer, M., von Hase, J., Volm, T., Brero, A., Kreth, G., Walter, J., Fischer, C., Solovei, I., Cremer, C. and Cremer, T. (2001). Non-random radial higher-order chromatin arrangements in nuclei of diploid human cells. *Chromosome Res.* **9**, 541-567.

Cremer, M., Küpper, K., Wagler, B., Wizelman, L., von Hase, J., Weiland, Y., Kreja, L., Diebold, J., Speicher, M. R. and Cremer, T. (2003). Inheritance of gene density-related higher order chromatin arrangements in normal and tumor cell nuclei. *J. Cell Biol.* **162**, 809-820.

Cremer, T., Cremer, M., Dietzel, S., Müller, S., Solovei, I. and Fakan, S. (2006). Chromosome territories: a functional nuclear landscape. *Curr. Opin. Cell Biol.* **18**, 307-316.

Croft, J. A., Bridger, J. M., Boyle, S., Perry, P., Teague, P. and Bickmore, W. A. (1999). Differences in the localization and morphology of chromosomes in the human nucleus. *J. Cell Biol.* **145**, 1119-1131.

Dimitrova, D. S. and Berezney, R. (2002). The spatio-temporal organization of DNA replication sites is identical in primary, immortalized and transformed mammalian cells. *J. Cell Sci.* **115**, 4037-4051.

Dutrillaux, B., Couturier, J., Richer, C. L. and Viegas-Pequignot, E. (1976). Sequence of DNA replication in 277 R- and Q-bands of human chromosomes using a BrdU treatment. *Chromosoma* **58**, 51-61.

Dyer, M. J., Nacheva, E., Fischer, P., Heward, J. M., Labastide, W. and Karpas, A. (1993). A new human T-cell lymphoma cell line (Karpas 384) of the T-cell receptor gamma/delta lineage with translocation t(7:14) (p13;q11.2). *Leukemia* **7**, 1047-1053.

Englmann, A., Clarke, L. A., Christan, S., Amaral, M. D., Schindelhauer, D. and Zink, D. (2005). The replication timing of CFTR and adjacent genes. *Chromosome Res.* **13**, 183-194.

Federico, C., Saccone, S., Andreozzi, L., Motta, S., Russo, V., Carels, N. and Bernardi, G. (2004). The pig genome: compositional analysis and identification of the gene-richest regions in chromosomes and nuclei. *Gene* **343**, 245-251.

Federico, C., Cantarella, C. D., Scavo, C., Saccone, S., Bed'hom, B. and Bernardi, G. (2005). Avian genomes: different karyotypes but a similar distribution of the GC-richest chromosome regions at interphase. *Chromosome Res.* **13**, 785-793.

Fiegler, H., Carr, P., Douglas, E. J., Burford, D. C., Hunt, S., Scott, C. E., Smith, J., Vetrie, D., Gorman, P., Tomlinson, I. P. et al. (2003). DNA microarrays for comparative genomic hybridization based on DOP-PCR amplification of BAC and PAC clones. *Genes Chromosomes Cancer* **36**, 361-374.

Foster, H. A. and Bridger, J. M. (2005). The genome and the nucleus: a marriage made by evolution. Genome organisation and nuclear architecture. *Chromosoma* **114**, 212-229.

Gilbert, N., Boyle, S., Fiegler, H., Woodfine, K., Carter, N. P. and Bickmore, W. A. (2004). Chromatin architecture of the human genome: gene-rich domains are enriched in open chromatin fibers. *Cell* **118**, 555-566.

Goetze, S., Mateos-Langerak, J., Gierman, H. J., de Leeuw, W., Giromus, O., Indemans, M. H., Koster, J., Ondrej, V., Versteeg, R. and van Driel, R. (2007). The three-dimensional structure of human interphase chromosomes is related to the transcriptome map. *Mol. Cell. Biol.* **27**, 4475-4487.

Gregory, S. G., Barlow, K. F., McLay, K. E., Kaul, R., Swarbreck, D., Dunham, A., Scott, C. E., Howe, K. L., Woodfine, K., Spencer, C. C. et al. (2006). The DNA sequence and biological annotation of human chromosome 1. *Nature* **441**, 315-321.

Habermann, F. A., Cremer, M., Walter, J., Kreth, G., von Hase, J., Bauer, K., Wienberg, J., Cremer, C., Cremer, T. and Solovei, I. (2001). Arrangements of macro- and microchromosomes in chicken cells. *Chromosome Res.* **9**, 569-584.

Hiratani, I., Leskovar, A. and Gilbert, D. M. (2004). Differentiation-induced replication-timing changes are restricted to AT-rich/long interspersed nuclear element (LINE)-rich isochores. *Proc. Natl. Acad. Sci. USA* **101**, 16861-16866.

Holmquist, G., Gray, M., Porter, T. and Jordan, J. (1982). Characterization of Giemsa dark- and light-band DNA. *Cell* **31**, 121-129.

Jeon, Y., Bekiranov, S., Karnani, N., Kapranov, P., Ghosh, S., MacAlpine, D., Lee, C., Hwang, D. S., Gingeras, T. R. and Dutta, A. (2005). Temporal profile of replication of human chromosomes. *Proc. Natl. Acad. Sci. USA* **102**, 6419-6424.

Karaman, M. W., Houck, M. L., Chemnick, L. G., Nagpal, S., Chawannakul, D., Sudano, D., Pike, B. L., Ho, V. V., Ryder, O. A. and Hacia, J. G. (2003). Comparative analysis of gene-expression patterns in human and African great ape cultured fibroblasts. *Genome Res.* **13**, 1619-1630.

Karnani, N., Taylor, C., Malhotra, A. and Dutta, A. (2007). Pan-S replication patterns and chromosomal domains defined by genome-tiling arrays of ENCODE genomic areas. *Genome Res.* **17**, 865-876.

Küpper, K., Kolbl, A., Biener, D., Dittrich, S., von Hase, J., Thormeyer, T., Fiegler, H., Carter, N. P., Speicher, M. R., Cremer, T. et al. (2007). Radial chromatin positioning is shaped by local gene density, not by gene expression. *Chromosoma* **116**, 285-386.

Lanctot, C., Cheutin, T., Cremer, M., Cavalli, G. and Cremer, T. (2007). Dynamic genome architecture in the nuclear space: regulation of gene expression in three dimensions. *Nat. Rev. Genet.* **8**, 104-115.

Mahy, N. L., Perry, P. E. and Bickmore, W. A. (2002). Gene density and transcription influence the localization of chromatin outside of chromosome territories detectable by FISH. *J. Cell Biol.* **159**, 753-763.

Mayr, C., Jasencakova, Z., Meister, A., Schubert, I. and Zink, D. (2003). Comparative analysis of the functional genome architecture of animal and plant cell nuclei. *Chromosome Res.* **11**, 471-484.

Misteli, T. (2005). Concepts in nuclear architecture. *BioEssays* **27**, 477-487.

Müller, S. (2006). Primate chromosome evolution. In *Genomic Disorders: The Genomic Basis of Disease* (ed. P. Stankiewicz and J. R. Lupski), pp. 133-152. Totowa, NJ: Humana Press.

Müller, S., Eder, V. and Wienberg, J. (2004). A nonredundant multicolor bar code as a screening tool for rearrangements in neoplasia. *Genes Chromosomes Cancer* **39**, 59-70.

Murmann, A. E., Gao, J., Encinosa, M., Gautier, M., Peter, M. E., Eils, R., Lichter, P. and Rowley, J. D. (2005). Local gene density predicts the spatial position of genetic loci in the interphase nucleus. *Exp. Cell Res.* **311**, 14-26.

Nakamura, H., Morita, T. and Sato, C. (1986). Structural organizations of replicon domains during DNA synthetic phase in the mammalian nucleus. *Exp. Cell Res.* **165**, 291-297.

Neusser, M., Schubel, V., Koch, A., Cremer, T. and Müller, S. (2007). Evolutionarily conserved, cell type and species-specific higher order chromatin arrangements in interphase nuclei of primates. *Chromosoma* **116**, 307-320.

Nogami, M., Nogami, O., Kagotani, K., Okumura, M., Taguchi, H., Ikemura, T. and Okumura, K. (2000). Intranuclear arrangement of human chromosome 12 correlates to large-scale replication domains. *Chromosoma* **108**, 514-522.

O'Keefe, R. T., Henderson, S. C. and Spector, D. L. (1992). Dynamic organization of DNA replication in mammalian cell nuclei: spatially and temporally defined replication of chromosome-specific alpha-satellite DNA sequences. *J. Cell Biol.* **116**, 1095-1110.

Postberg, J., Alexandrova, O., Cremer, T. and Lipps, H. J. (2005). Exploiting nuclear duality of ciliates to analyse topological requirements for DNA replication and transcription. *J. Cell Sci.* **118**, 3973-3983.

Raghuraman, M. K., Winzeler, E. A., Collingwood, D., Hunt, S., Wodicka, L., Conway, A., Lockhart, D. J., Davis, R. W., Brewer, B. J. and Fangman, W. L. (2001). Replication dynamics of the yeast genome. *Science* **294**, 115-121.

Saccone, S., Federico, C. and Bernardi, G. (2002). Localization of the gene-richest and the gene-poorest isochores in the interphase nuclei of mammals and birds. *Gene* **300**, 169-178.

Sadoni, N., Langer, S., Fauth, C., Bernardi, G., Cremer, T., Turner, B. M. and Zink, D. (1999). Nuclear organization of mammalian genomes. Polar chromosome territories build up functionally distinct higher order compartments. *J. Cell Biol.* **146**, 1211-1226.

Schermelleh, L., Solovei, I., Zink, D. and Cremer, T. (2001). Two-color fluorescence labeling of early and mid-to-late replicating chromatin in living cells. *Chromosome Res.* **9**, 77-80.

Schubeler, D., Scalzo, D., Kooperberg, C., van Steensel, B., Delrow, J. and Groudine, M. (2002). Genome-wide DNA replication profile for Drosophila melanogaster: a link between transcription and replication timing. *Nat. Genet.* **32**, 438-442.

Schwaiger, M. and Schubeler, D. (2006). A question of timing: emerging links between transcription and replication. *Curr. Opin. Genet. Dev.* **16**, 177-183.

Solovei, I., Walter, J., Cremer, M., Habermann, F., Schermelleh, L. and Cremer, T. (2002). FISH on three-dimensionally preserved nuclei. In *FISH: A Practical Approach* (ed. B. Beatty, S. Mai and J. Squire), pp. 119-157. Oxford: Oxford University Press.

Taylor, J. H., Woods, P. S. and Hughes, W. L. (1957). The organization and duplication of chromosomes as revealed by autoradiographic studies using tritium-labeled thymidine. *Proc. Natl. Acad. Sci. USA* **43**, 122-128.

Visser, A. E., Eils, R., Jauch, A., Little, G., Bakker, P. J., Cremer, T. and Aten, J. A. (1998). Spatial distributions of early and late replicating chromatin in interphase chromosome territories. *Exp. Cell Res.* **243**, 398-407.

Volpi, E. V., Chevret, E., Jones, T., Vatcheva, R., Williamson, J., Beck, S., Campbell, R. D., Goldsworthy, M., Powis, S. H., Ragoussis, J. et al. (2000). Large-scale chromatin organization of the major histocompatibility complex and other regions of human chromosome 6 and its response to interferon in interphase nuclei. *J. Cell Sci.* **113**, 1565-1576.

Weber, B., Schempp, W. and Wiesner, H. (1986). An evolutionary conserved early replicating segment on the sex chromosomes of man and the great apes. *Cytogenet. Cell Genet.* **43**, 72-78.

White, E. J., Emanuelsson, O., Scalzo, D., Royce, T., Kosak, S., Oakeley, E. J., Weissman, S., Gerstein, M., Groudine, M., Snyder, M. et al. (2004). DNA replication-timing analysis of human chromosome 22 at high resolution and different developmental states. *Proc. Natl. Acad. Sci. USA* **101**, 17771-17776.

Williams, R. R., Broad, S., Sheer, D. and Ragoussis, J. (2002). Subchromosomal positioning of the epidermal differentiation complex (EDC) in keratinocyte and lymphoblast interphase nuclei. *Exp. Cell Res.* **272**, 163-175.

Woodfine, K., Fiegler, H., Beare, D. M., Collins, J. E., McCann, O. T., Young, B. D., Debernardi, S., Mott, R., Dunham, I. and Carter, N. P. (2004). Replication timing of the human genome. *Hum. Mol. Genet.* **13**, 191-202.

Woodfine, K., Beare, D. M., Ichimura, K., Debernardi, S., Mungall, A. J., Fiegler, H., Collins, V. P., Carter, N. P. and Dunham, I. (2005). Replication timing of human chromosome 6. *Cell Cycle* **4**, 172-176.

Yokota, H., van den Engh, G., Hearst, J. E., Sachs, R. K. and Trask, B. J. (1995). Evidence for the organization of chromatin in megabase pair-sized loops arranged along a random walk path in the human G0/G1 interphase nucleus. *J. Cell Biol.* **130**, 1239-1249.

Zink, D. (2006). The temporal program of DNA replication: new insights into old questions. *Chromosoma* **115**, 273-287.

Table S1. Mapping positions, genomic properties and replication timing of all large-insert clones used as FISH probes in this study, either as pools as indicated in A-E, as subsets thereof or as individual probes. The large-insert clone ID refers to the abbreviation used throughout the text. The mapping position was derived from the NCBI 36 assembly (www.ensembl.org). [a)] The replication timing was previously determined by array-CGH (Woodfine et al., 2004). Each clone was assigned to an isochore according to the previously published isochore map of the human genome (Costantini et al., 2006). Isochores [b)] are DNA segments with an internal variation in [c)] %GC content below the full variation of the GC content in the entire human genome, [d)] The local gene density was determined based on the available information on 'known genes' (NCBI 36 assembly; www.ensembl.org) for a 2 Mb window, 1 Mb upstream and 1 Mb downstream of the center of each clone.

(A) Chromosome 1-22 and X large-insert clone pools representing early-replicating (green) and late-replicating (red) loci, each one clone per chromosome, if available

Clone ID	1 Mb array ID	Clone name	Chr.	Position (bp)	Clone length (bp)	Replication timing [a)]	Isochore position (Mbp) [b)]	% GC in isochore [c)]	Genes ± 1 Mbp [d)]
1e	dJ144C9	RP1-144C9	1	27575323-27652644	77322	2.03	24.9-28.3	48.1	65
1l	bA552K17	RP11-552K17	1	194520170-194617850	97681	1.03	194.5-194.9	38.40	11
2-1e	bA83M8	RP11-83M8	2	10189946-10392995	203050	1.97	10.1-11.2	48.7	34
2-3l	bA458O14	RP11-458O14	2	79819775-79920395	100621	1.04	78.9-80.9	38.60	13
3e	bA78O10	RP11-78O10	3	49843917-49994333	150417	2.04	49-50.1	49.1	74
3l	bA90M7	RP11-90M7	3	164366661-164516629	149969	1.05	162.8-169.2	35.1	1
4e	bA572O17	RP11-572O17	4	1595351-1782573	187223	1.96	0.5-4.3	51.9	52
4l	bA347K3	RP11-347K3	4	189700508-189778943	78436	0.98	189.6-190.7	38.8	11
5-4l	bA170P5	RP11-170P5	5	165677723-165841050	163328	1.06	165.6-166.7	38.1	4
6e	dJ34F7	RP1-34F7	6	32031967-32200774	168808	1.99	31.6-32.3	51.9	109
6l	bA21G12	RP11-21G12	6	93190239-93225251	35013	1.09	92.1-97.2	35.1	6
7-3e	bA450O3	RP11-450O3	7	72073705-72269192	195488	1.94	71.7-73.5	49.9	48

7l	bA343J14	bA343J14	7	78310705-78485567	174863	1.05	77.7-79.4	35.8	8
8e	bA446E9	RP11-446E9	8	57012703-57129759	117057	1.92	56.9-57.7	41.3	22
8l	bA75P13	RP11-75P13	8	34287721-34455078	167358	1.05	33.8-37.1	38.2	12
9e	bA570D4	RP11-570D4	9	113691272-113781581	90310	1.92	113.5-113.8	42.9	26
9l	bA264J11	RP11-264J11	9	28670842-28755649	84808	1.05	28.2-31.9	35.20	1
10e	bA122K13	RP11-122K13	10	134955982-135072292	116311	1.92	133.8-135.1	56.5	38
10l	bA428N21	RP11-428N21	10	68138624-68290770	152147	1.02	65.7-68.9	35.7	6
11e	bA231P15	RP11-231P15	11	62241256-62406841	165586	1.92	61.9-62.6	49.0	79
11l	bA324K6	RP11-324K6	11	37673711-37779927	106217	1.07	37-39.3	35.4	0
12e	bA474N8	RP11-474N8	12	55578149-55750146	171998	2.01	55.6-56.6	48.3	98
12l	bA268A19	RP11-268A19	12	80263369-80282240	18872	1.11	79.1-81.5	35.5	13
13l	bA275J18	RP11-275J18	13	88476233-88642741	166509	1.09	80.2-90.1	34.6	4
14e	bA463C8	RP11-463C8	14	76653300-76831630	178331	1.93	76.3-76.9	49.0	34
14l	bA168D12	RP11-168D12	14	41353854-41500293	146440	0.99	39.5-43.9	34.7	1
15e	bA414J4	RP11-414J4	15	72768830-72953361	184532	2.00	72.5-73.9	48.9	58
15l	bA215J7	RP11-215J7	15	52652476-52815253	162778	1.12	52.2-52.8	35.9	15
16e	bA2C24	RP11-2C24	16	30539890-30747839	207950	1.93	26.9-30.8	49	101
16l	bA467L24	RP11-467L24	16	62921648-63071733	150086	1.05	61.8-63.2	36.2	1
17-5e	bA141D15	RP11-141D15	17	73636218-73813841	177624	2.11	73.6-74	54.0	47
18e	bA61J14	RP11-61J14	18	54567090-54747580	180491	2.03	52.8-55.8	43.1	21
18l	bA25O3	RP11-25O3	18	47958320-48119508	161189	1.05	47.1-48.6	38.70	6
19e	bA521I20	RP11-521I20	19	54525652-54718270	192619	2.15	53.3-55.2	52.3	114
20e	bB152O15	RP13-152O15	20	62108686-62284676	175991	2.38	59.6-62.5	55.0	54
21e	bA113F1	RP11-113F1	21	42507308-42689289	181982	1.98	41.4-43.5	49.0	36
21l	bA509A1	RP11-509A1	21	21128294-21149667	21374	1.09	18.4-25.6	35.10	5

22e	dJ76B20	RP1-76B20	22	28379384-28551065	171682	1.95	27.7-29.9	48.0	83
Xe	bA54I20	RP11-54I20	X	152359266-152538562	179297	1.98	152.2-152.8	55.8	76
Xl	dA22P16	RP6-22P16	X	66474359-66577725	103367	1.07	66.3-66.5	36.7	6

(B) Chromosome-2-specific large-insert clone pools representing early-replicating (green) and late-replicating (red) loci

Clone ID	**1 Mb array ID**	**Clone name**	**Chr.**	**Position (bp)**	**Clone length (bp)**	**Replication timing** [a)]	**Isochore position (Mbp)** [b)]	**% GC in isochore** [c)]	**Genes ± 1 Mbp** [d)]
2-1e	bA83M8	RP11-83M8	2	10189946-10392995	203050	1.97	10.1-11.2	48.7	34
2-2l	bA419E14	RP11-419E14	2	78739646-78927111	187466	1.12	76.1-78.9	35.30	12
2-3l	bA458O14	RP11-458O14	2	79819775-79920395	100621	1.04	78.9-80.9	38.60	13
2-4e	bA139J6	RP11-139J6	2	96130286-96151127	20842	2.00	96.1-97.1	49	47
2-5l	bA339P1	RP11-339P1	2	116380901-116514763	133863	1.08	115.3-118.1	36.60	13
2-6l	bA272E3	RP11-272E3	2	165238465-165429463	190999	1.11	162.9-166.3	36.00	12
2-7e	bA419H23	RP11-419H23	2	231787899-231964428	176530	2.02	231.7-232	42.9	40

(C) Chromosome-5-specific large-insert clone pools representing late-replicating (red) loci

Clone ID	**1 Mb array ID**	**Clone name**	**Chr.**	**Position (bp)**	**Clone length (bp)**	**Replication timing** [a)]	**Isochore position (Mbp)** [b)]	**% GC in isochore** [c)]	**Genes ± 1 Mbp** [d)]
5-1l	bA192H6	RP11-192H6	5	25187395-25333181	145787	1.10	23.2-31.6	35.30	4
5-2l	bA153B10	RP11-153B10	5	113303877-113366022	62146	1.13	113.1-114.4	38.00	7
5-3l	bA11P11	RP11-11P11	5	121061464-121226480	165017	1.13	119.2-121.4	35.50	11
5-4l	bA170P5	RP11-170P5	5	165677723-165841050	163328	1.06	165.6-166.7	38.10	4

(D) Chromosome-7-specific large-insert clone pools representing early-replicating (green) and late-replicating (red) loci

Clone ID	**1 Mb array ID**	**Clone name**	**Chr.**	**Position (bp)**	**Clone length (bp)**	**Replication timing** [a)]	**Isochore position (Mbp)** [b)]	**% GC in isochore** [c)]	**Genes ± 1 Mbp** [d)]

7-1e	bA106E3	RP11-106E3	7	2607390-2657138	49749	2.00	2.5-3.1	47.8	22
7-2l	bA512E16	RP11-512E16	7	14128072-14279388	151317	1.11	12.7-16.1	35.60	3
7-3e	bA450O3	RP11-450O3	7	72073705-72269192	195488	1.94	71.7-73.5	49.9	48
7-4l	dJ1057M1	RP5-1057M1	7	79539131-79644969	105839	1.06	79.4-80.2	36.40	8
7-5l	bA242J14	RP11-242J14	7	83230804-83414012	183209	1.11	80.5-86	35.00	6
7-6l	dJ558L10	RP4-558L10	7	145959491-146102540	143050	1.11	144.1-146.6	36.10	3

(E) Chromosome-17-specific large-insert clone pools representing early-replicating (green) loci

Clone ID	**1 Mb array ID**	**Clone name**	**Chr.**	**Position (bp)**	**Clone length (bp)**	**Replication timing** [a)]	**Isochore position (Mbp)** [b)]	**% GC in isochore** [c)]	**Genes ± 1 Mbp** [d)]
17-1e	bA216P6	RP11-216P6	17	800495-1008155	207661	1.91	0.8-1.1	54.1	48
17-2e	bA524F11	RP11-524F11	17	17338138-17521471	183334	1.98	17.3-17.7	53.9	62
17-3e	bA189D22	RP11-189D22	17	17942719-18110985	168267	2.10	17.9-18.1	53.3	67
17-4e	bK58E17	Cancer3C7	17	33964845-34251503	286659	1.97	33.8-34.2	53.1	50
17-5e	bA58O9	RP11-58O9	17	35754712-35920945	166234	1.96	35-36	49.2	95
17-6e	bA141D15	RP11-141D15	17	73636218-73813841	177624	2.11	73.6-74	54	47
17-7e	bA567O16	RP11-567O16	17	78311474-78374827	63354	1.99	76.4-78.8	55.8	52

Table S2. Statistical analysis of 3RRD (relative radial distribution) and eADS (absolute distance to surface) evaluations obtained from 3D-FISH experiments (ARR=average relative radius in %, 0%=nuclear centre, 100%=nuclear border; ADS= absolute distance to surface in nm; n=evaluated nuclei; sem=standard error of the mean, *P*-values in green=distribution difference statistically significant, *P*-values in blue=distribution difference statistically not significant).

(A) Chromosome 1-22 and X large-insert clone probe set

ADS nucleus

Cell line	**n**	**Early clones: ADS ±sem**	**Late clones: ADS ±sem**	**Δ ADS**	***P* (U-test)**
Human fibroblasts	21	989 nm ±3.2 nm	869 nm ±3.6 nm	120 nm	$P = 0.039$
Mel Juso	22	1703 nm ±3.1 nm	1364 nm ±3.7 nm	339 nm	$P < 0.001$
SW620	22	1640 nm ±2.9 nm	1255 nm ±3.3 nm	385 nm	$P < 0.001$

ARR nucleus

Cell line	**n**	**Early clones: ARR ±sem**	**Late clones: ARR ±sem**	**Δ ARR**	***P* (U-test)**
Human fibroblasts	21	63.1% ±0.4%	61.2% ±0.4%	–1.9%	$P = 0.246$
Mel Juso	22	60.0% ±0.4%	61.7% ±0.4%	1.7%	$P = 0.269$
SW620	22	58.9% ±0.4%	63.8% ±0.4%	4.9%	$P = 0.007$

(B) Chromosome 1-22 and X large-insert clone probe set combined with double pulse labeling for the delineation of early and late replication foci

ADS nucleus

Cell line	**n**	**Early clones: ADS ±sem**	**Late clones: ADS ±sem**	**Δ ADS**	***P* (U-test)**
Human fibroblasts	8	988 nm ±5.1 nm	698 nm ±5.5 nm	–290 nm	$P = 0.038$

Cell line	**n**	**Early Foci: ADS ±sem**	**Late Foci: ADS ±sem**	**Δ ADS**	***P* (U-test)**
Human fibroblasts	8	906 nm ±4.9 nm	995 nm ±5.0 nm	–89 nm	$P = 0.234$

Cell line	**n**	**Early clones: ADS ±sem**	**Early Foci: ADS ±sem**	**Δ ADS**	***P* (U-test)**
Human fibroblasts	8	988 nm ±5.1 nm	906 nm ±4.9 nm	82 nm	$P = 0.279$

Cell line	**n**	**Late clones: ADS ±sem**	**Late Foci: ADS ±sem**	**Δ ADS**	***P* (U-test)**
Human fibroblasts	8	698 nm ±5.5 nm	995 nm ±5.0 nm	–297 nm	$P = 0.038$

Cell line	**n**	**Counterstain: ADS ±sem**	**Early Foci: ADS ±sem**	**Δ ADS**	***P* (U-test)**
Human fibroblasts	8	577 nm ±3.7 nm	906 nm ±4.9 nm	–329 nm	$P = 0.005$

Cell line	**n**	**Counterstain: ADS ±sem**	**Early clones: ADS ±sem**	**Δ ADS**	***P* (U-test)**
Human fibroblasts	8	577 nm ±3.7 nm	988 nm ±5.1 nm	–411 nm	$P = 0.003$

Cell line	**n**	**Counterstain: ADS ±sem**	**Late Foci: ADS ±sem**	**Δ ADS**	***P* (U-test)**
Human fibroblasts	8	577 nm ±3.7 nm	995 nm ±5.0 nm	–418 nm	$P = 0.003$

Cell line	**n**	**Counterstain: ADS ±sem**	**Late clones: ADS ±sem**	**Δ ADS**	***P* (U-test)**
Human fibroblasts	8	577 nm ±3.7 nm	698 nm ±5.5 nm	–121 nm	$P = 0.161$

C) Chromosome 2 large-insert clone probe set

ARR nucleus

Cell line	**n**	**Early clones: ARR**	**Late clones: ARR**	**Δ ARR**	***P* (U-test)**

		±sem	±sem		
Human fibroblasts	20	64.4% ±0.99%	68.3% ±0.94%	3.9%	$P = 0.239$
Human lymphoblastoids	22	59.3% ±0.84%	62.8% ±1.06%	3.5%	$P = 0.330$
Gorilla lymphoblastoids	25	60.7% ±0.76%	64.3% ±0.91%	3.6%	$P = 0.140$

Cell line	**n**	**Early clones human ly: ARR ±sem**	**Early clones gorilla ly: ARR ±sem**	**Δ ARR**	***P* (U-test)**
Human vs. gorilla lymphoblastoids	22 25	59.3% ±0.84%	60.7% ±0.76%	–1.4%	$P = 0.072$

Cell line	**n**	**Late clones human ly: ARR ±sem**	**Late clones gorilla ly: ARR ±sem**	**Δ ARR**	***P* (U-test)**
Human vs. gorilla lymphoblastoids	22 25	62.8% ±1.06%	64.3% ±0.91%	–1.5%	$P = 0.502$

Cell line	**n**	**Early clones human fib: ARR ±sem**	**Early clones human ly: ARR ±sem**	**Δ ARR**	***P* (U-test)**
Human fibroblasts vs. human lymphoblastoids	22 25	64.4% ±0.99%	59.3% ±0.84%	5.1%	$P = 0.085$

Cell line	**n**	**Late clones human fib: ARR ±sem**	**Late clones human ly: ARR ±sem**	**Δ ARR**	***P* (U-test)**
Human fibroblasts vs. human lymphoblastoids	22 25	68.3% ±0.94%	62.8% ±1.06%	5.5%	$P = 0,252$

Cell line	**n**	**clone 2-3l: ARR ±sem**	**clone 2-6l: ARR ±sem**	**Δ ARR**	***P* (U-test)**
Human fibroblasts	20	60.2% ±1.72%	70.3% ±0.45%	10.1%	$P = 0.002$

ADS chromosome 2 territory

Cell line	**n**	**Early clones: ADS ±sem**	**Late clones: ADS ±sem**	**Δ ADS**	***P* (U-test)**
Human fibroblasts	26	377 nm ±3.7 nm	500 nm ±2.9 nm	–123 nm	$P = 0.134$
Human lymphoblastoids	16	330 nm ±4.4 nm	300 nm ±3.7 nm	+30 nm	$P = 0.734$

(D) Chromosome 5 and 17 BAC probe set

ARR nucleus

Cell line	**n**	**Early clones chr. 17: ARR ±sem**	**Late clones chr. 5: ARR ±sem**	**Δ ARR**	***P* (U-test)**
Human fibroblasts	24	54.8% ±0.79%	70.4%±0.99%	15.6%	$P < 0.001$
Human lymphoblastoids	21	40.9% ±0.72%	66.8%±1.04%	25.9%	$P < 0.001$
Gorilla fibroblasts	22	58.8% ±0.76%	66.3% ±0.81%	7.5%	$P = 0.004$
Gorilla lymphoblastoids	20	50.9% ±0.75%	66.1% ±1.04%	15.2%	$P < 0.001$
Gibbon lymphoblastoids	22	51.9% ±0.84%	68.5% ±0.91	16.6%	$P < 0.001$

Cell line	**n**	**Early clones chr. 17: ARR ±sem**	**Early clones der(17): ARR ±sem**	**Δ ARR**	***P* (U-test)**
Mel Juso	21	57.7 ±0.83	51.7 ±0.82	6.0%	$P = 0.027$

Cell line	**n**	**Chr. 17 territory: ARR ±sem**	**der(17) territory: ARR ±sem**	**Δ ARR**	***P* (U-test)**
Mel Juso	21	59.3±0.61	64.7±0.47	5.4%	$P =0.019$

Cell line	**n**	**clone 7-1e: ARR ±sem**	**clones 7-2l/5-1l: ARR ±sem**	**Δ ARR**	***P* (U-test)**

SW620 t(5p7p)	18	60.6% ±2.19%	75.4% ±1.65%	14.8%	$P = 0.009$
SW620 chr. 5 and 7	20	60.7% ±1.31%	69.7% ±1.06%	9.0%	$P = 0.015$

Cell line	**n**	**clone 7-1e: ARR ±sem**	**clone 7-1e: ARR ±sem**	**Δ ARR**	***P* (U-test)**
SW620 t(5p7p) vs. chr. 5 and 7	18 20	60.6% ±2.19%	60.7% ±1.31%	–0.1%	$P = 0.783$

Cell line	**n**	**clones 7-2l/5-1l: ARR ±sem**	**clones 7-2l/5-1l: ARR ±sem**	**Δ ARR**	***P* (U-test)**
SW620 t(5p7p) vs. chr. 5 and 7	18 20	75.4% ±1.65%	69.7% ±1.06%	5.7%	$P = 0.027$

ADS chromosome 5 and 17 territory

Cell line	**n**	**Early clones chr. 17: ADS ±sem**	**Late clones chr. 5: ADS ±sem**	**Δ ADS**	***P* (U-test)**
Human fibroblasts	25	178 nm ±3.5 nm		n.d.	n.d.
	29		634 nm ±3.7 nm		n.d.
Gorilla fibroblasts t(5;17) large	23	469 nm ±3.3 nm	806 nm ±3.2 nm	–377 nm	$P < 0.001$
Gorilla fibroblasts t(5;17) small	23	310 nm ±4.3 nm	691 nm ±3.6 nm	–381 nm	$P < 0.001$

(E) Chromosome 7 BAC probe set

ARR nucleus

Cell line	**n**	**Early clones: ARR ±sem**	**Late clones: ARR ±sem**	**Δ ARR**	***P* (U-test)**
Human fibroblasts	20	54.4% ±1.01%	67.5% ±1.01%	13.1%	$P = 0.026$
Human lymphoblastoids	22	56.9% ±0.88%	68.4% ±0.90%	11.5%	$P < 0.001$
Orangutan lymphoblastoids	20	50.6% ±1.03%	69.7% ±1.03%	19.1%	$P < 0.001$
Gibbon lymphoblastoids	20	54.4% ±1.01%	67.5% ±1.01%	13.1%	$P < 0.001$
Karpas 384 chr. 7	22	64.3% ±1.01%	78.0% ±0.95%	13.7%	$P < 0.001$
Karpas 384 der(7)	22	62.5% ±1.34%	70.9% ±1.35%	8.4%	$P = 0.002$

Cell line	**n**	**Early clones: ARR ±sem**	**Early clones: ARR ±sem**	**Δ ARR**	***P* (U-test)**
Karpas 384 der(7) vs. chr. 7	22	62.5% ±1.34%	64.3% ±1.01%	–1.8%	$P = 0.972$

Cell line	**n**	**Late clones: ARR ±sem**	**Late clones: ARR ±sem**	**Δ ARR**	***P* (U-test)**
Karpas 384 der(7) vs. chr. 7	22	70.9% ±1.35%	78.0% ±0.95%	–7.1%	$P = 0.065$

Cell line	**n**	**clone 7-1e: ARR ±sem**	**clone 7-2l: ARR ±sem**	**Δ ARR**	***P* (U-test)**
Mel Juso iso(7p)	**20**	64.5% ±1.24%	67.5% ±0.72%	3.0%	$P = 0.032$
Mel Juso chr. 7	**20**	63.0% ±1.43	65.0% ±0.72%	2.0%	$P = 0.164$

Cell line	**n**	**clone 7-1e: ARR ±sem**	**clone 7-1e: ARR ±sem**	**Δ ARR**	***P* (U-test)**
Mel Juso iso(7p) vs chr. 7	**20**	64.5% ±1.24%	63.0% ±1.43	1.5%	$P = 0.797$

Cell line	**n**	**clone 7-2l: ARR ±sem**	**clone 7-2l: ARR ±sem**	**Δ ARR**	***P* (U-test)**
Mel Juso iso(7p) vs chr. 7	**20**	67.5% ±0.72%	65.0% ±0.72%	2.5%	$P = 0.441$

Cell line	**n**	**7-1e: ARR ±sem**	**7-2l: ARR ±sem**	**Δ ARR**	***P* (U-test)**
Human fibroblasts	22	60.6% ±1.52%	64.3% ±1.55%	–3.7%	$P = 0.614$

Cell line	n	7-2l: ARR ±sem	7-3e: ARR ±sem	Δ ARR	*P* (U-test)
Human fibroblasts	22	64.3% ±1.55%	64.2% ±1.59%	0.1%	$P = 0.952$

Cell line	n	7-3e: ARR ±sem	7-4l: ARR ±sem	Δ ARR	*P* (U-test)
Human fibroblasts	22	64.2% ±1.59%	66.4% ±1.49%	–2.2%	$P = 0.653$

Cell line	n	7-4l: ARR ±sem	7-6l: ARR ±sem	Δ ARR	*P* (U-test)
Human fibroblasts	22	66.4% ±1.49%	75.6% ±1.61%	–9.2%	$P = 0.025$

Cell line	n	7-1e: ARR ±sem	7-3l: ARR ±sem	Δ ARR	*P* (U-test)
Human fibroblasts	22	60.6% ±1.52%	64.2% ±1.59%	–4.0%	$P = 0.459$

Cell line	n	7-1e: ARR ±sem	7-4l: ARR ±sem	Δ ARR	*P* (U-test)
Human fibroblasts	22	60.6% ±1.52%	66.4% ±1.49%	–5.8%	$P = 0.201$

Cell line	n	7-1e: ARR ±sem	7-6l: ARR ±sem	Δ ARR	*P* (U-test)
Human fibroblasts	22	60.6% ±1.52%	75.6% ±1.61%	–15.0%	$P = 0.001$

Cell line	n	7-2l: ARR ±sem	7-4l: ARR ±sem	Δ ARR	*P* (U-test)
Human fibroblasts	22	64.3% ±1.55%	66.4% ±1.49%	–1.9%	$P = 0.489$

Cell line	n	7-2l: ARR ±sem	7-6l: ARR ±sem	Δ ARR	*P* (U-test)
Human fibroblasts	22	64.3% ±1.55%	75.6% ±1.61%	–11.3%	$P = 0.019$

Cell line	n	7-3e: ARR ±sem	7-6l: ARR ±sem	Δ ARR	*P* (U-test)
Human fibroblasts	22	64.2% ±1.59%	75.6% ±1.61%	–11.4%	$P = 0.013$

Cell line	n	7-1e: ARR ±sem	7-2l: ARR ±sem	Δ ARR	*P* (U-test)
Orangutan fibroblasts	22	60.4% ±1.49%	71.9% ±1.52%	–11.5%	$P = 0.008$

Cell line	n	7-2l: ARR ±sem	7-3e: ARR ±sem	Δ ARR	*P* (U-test)
Orangutan fibroblasts	22	71.9% ±1.52%	65.1% ±1.97%	6.8%	$P = 0.130$

Cell line	n	7-3e: ARR ±sem	7-4l: ARR ±sem	Δ ARR	*P* (U-test)
Orangutan fibroblasts	22	65.1% ±1.97%	74.0% ±1.59%	–9.1%	$P = 0.054$

Cell line	n	7-4l: ARR ±sem	7-6l: ARR ±sem	Δ ARR	*P* (U-test)
Orangutan fibroblasts	22	74.0% ±1.59%	79.2% ±1.86%	–5.2%	$P = 0.330$

Cell line	n	7-1e: ARR ±sem	7-3e: ARR ±sem	Δ ARR	*P* (U-test)
Orangutan fibroblasts	22	60.4% ±1.49%	65.1% ±1.97%	–4.7%	$P = 0.321$

Cell line	n	7-1e: ARR ±sem	7-4l: ARR ±sem	Δ ARR	*P* (U-test)
Orangutan fibroblasts	22	60.4% ±1.49%	74.0% ±1.59%	–13.6%	$P = 0.003$

Cell line	n	7-1e: ARR ±sem	7-6l: ARR ±sem	Δ ARR	*P* (U-test)
Orangutan fibroblasts	22	60.4% ±1.49%	79.2% ±1.86%	-18.8%	$P = 0.003$

Cell line	n	7-2e: ARR ±sem	7-4l: ARR ±sem	Δ ARR	*P* (U-test)
Orangutan fibroblasts	22	71.9% ±1.52%	74.0% ±1.59%	–2.1%	$P = 0.580$

Cell line	n	7-2l: ARR ±sem	7-6l: ARR ±sem	Δ ARR	*P* (U-test)
Orangutan fibroblasts	22	71.9% ±1.52%	79.2% ±1.86%	–7.3%	$P = 0.176$

Cell line	n	7-3l: ARR ±sem	7-6l: ARR ±sem	Δ ARR	*P* (U-test)
Orangutan fibroblasts	22	65.1% ±1.97%	79.2% ±1.86%	–14.1%	$P = 0.027$

Cell line	n	7-1e HSA: ARR ±sem	7-1e PPY: ARR ±sem	Δ ARR	*P* (U-test)
Human vs. Orangutan fibroblasts	**22**	60.6% ±1.52%	60.4% ±1.49%	0.2%	$P = 0.808$

Cell line	n	7-2l HSA: ARR ±sem	7-2l PPY: ARR ±sem	Δ ARR	*P* (U-test)
Human vs. Orangutan fibroblasts	**22**	64.3% ±1.52%	71.9% ±1.45%	–7.6%	$P = 0.082$

Cell line	n	7-3e HSA: ARR ±sem	7-3e PPY: ARR ±sem	Δ ARR	*P* (U-test)
Human vs. Orangutan fibroblasts	**22**	64.2% ±1.59%	65.1% ±1.97%	–0.9%	$P = 0.837$

Cell line	n	7-4l HSA: ARR ±sem	7-4l PPY: ARR ±sem	Δ ARR	*P* (U-test)
Human vs. Orangutan fibroblasts	**22**	66.4% ±1.49%	74.0% ±1.52%	–7.6%	$P = 0.070$

Cell line	n	7-6l HSA: ARR ±sem	7-6l PPY: ARR ±sem	Δ ARR	*P* (U-test)
Human vs. Orangutan fibroblasts	**22**	75.6% ±1.61%	79.2% ±1.86%	–3.6%	$P = 0.602$

ADS chromosome 7 territory

Cell line	n	Early clones: ADS ±sem	Late clones chr. 5: ADS ±sem	Δ ADS	*P* (U-test)
Human fibroblasts	28	333 nm ±3.6 nm	369 nm ±3.4 nm	36 nm	$P = 0.812$
Human lymphoblastoids	24	581 nm ±3.3 nm	622 nm ±3.6 nm	41 nm	$P = 0.743$
Orangutan lymphoblastoids	24	190 nm ±4.3 nm	638 nm ±3.4 nm	448 nm	$P < 0.001$